https://doi.org/10.5194/tc-2023-54
Preprint. Discussion started: 8 May 2023

The Cryosphere Discussions
Open Access
EGU

Early Holocene ice on the Begguya plateau (Mt. Hunter, Alaska) revealed by ice core ^{14}C age constraints

Ling Fang[1,$], Theo M. Jenk[1,3*], Dominic Winski[4], Karl Kreutz[4], Hanna L. Brooks[4], Emma Erwin[4], Erich Osterberg[5], Seth Campbell[4], Cameron Wake[6], Margit Schwikowski[1,2,3]

[1]Laboratory for Environmental Chemistry, Paul Scherrer Institute, CH-5232 Villigen PSI, Switzerland

[2]Department of Chemistry and Biochemistry, University of Bern, CH-3012 Bern, Switzerland

[3]Oeschger Centre for Climate Change Research, University of Bern, CH-3012 Bern, Switzerland

[4]Climate Change Institute and School of Earth and Climate Science, University of Maine, Orono, Maine, 04469, USA.

[5]Deparment of Earth Sciences, Dartmouth College, Hanover, NH 03755

[6]Institute for the Study of Earth, Oceans, and Space, University of New Hampshire, Durham, NH 03824

[$]Present address: Shaanxi Key Laboratory of Earth Surface System and Environmental Carrying Capacity, Urban and Environmental Sciences department, Northwest University, Xi'an 710127, China.

*Corresponding author

https://doi.org/10.5194/tc-2023-54
Preprint. Discussion started: 8 May 2023


The Cryosphere Discussions
Open Access
EGU

Abstract

Investigating North Pacific climate variability during warm intervals prior to the Common Era can improve our understanding of the behavior of ocean-atmosphere teleconnections between low latitudes and the Arctic under future warming scenarios. However, most of the existing ice core records from the Alaska/Yukon region only allow access to climate information covering the last few centuries. Here we present a surface-to-bedrock age scale for a 210-meter long ice core recovered in 2013 from the summit plateau of Begguya (Mt. Hunter; Denali National Park, Central Alaska). Combining dating by annual layer counting with absolute dates from micro-radiocarbon dating, a continuous chronology for the entire ice core archive was established using an ice flow model. Calibrated ^{14}C ages from the deepest section (209.1 m, 7.7 to 9.0 ka cal BP) indicate that basal ice on Begguya is at least of early Holocene origin. A series of samples from a shallower depth interval (199.8 to 206.6 m) were dated with near uniform ^{14}C ages (3 to 5 ka cal BP). Our results suggest this may be related to an increase in annual net snow accumulation rates over this period following the Northern Hemisphere Holocene Climate Optimum (around 8 to 5 ka BP). With absolute dates constraining the timescale for the last > 8 ka, this paleo archive will allow future investigations of Holocene climate and the regional evolution of spatial and temporal changes in atmospheric circulation and hydroclimate in the North Pacific.

https://doi.org/10.5194/tc-2023-54
Preprint. Discussion started: 8 May 2023

1 Introduction

Arctic surface temperatures have increased more than twice as fast as global temperature during the early 20th century and since the 1970s (Bengtsson 2004, Tokinaga et al. 2017, Svendsen et al. 2018). Recent modeling results suggest that during the early 20th century, as the Pacific Decadal Oscillation (PDO) transitioned to a positive phase, there was a concomitant deepening of the Aleutian Low that warmed the Arctic through poleward low-level advection of extratropical air (Svendsen et al. 2018). The impact of Pacific multi-decadal variability on Arctic warming has considerable implications for sea ice extent (Screen and Francis 2016), and hence the possible linkage between Arctic amplification, sea ice loss, and enhanced mid-latitude winter variability (Cohen et al. 2014, Francis et al. 2017, Cohen et al. 2018, Screen et al. 2018, Blackport et al. 2019, Cohen et al. 2019). Whether the present positive PDO conditions will persist and contribute to Arctic warming at an even higher rate in the future remains a fundamental question (Svendsen et al. 2018). A longer-term perspective on Pacific decadal variability and the teleconnection between the tropical Pacific, North Pacific, and the Arctic, particularly during warm intervals in the Holocene outside those captured in the instrumental record, would be an important contribution to this problem (e.g., Park et al. 2019). High-mountain ice cores in the North Pacific region have the advantage of sampling atmospheric moisture (e.g., snow), aerosol deposition, and preserving physical characteristics (e.g., melt), all of which can be related to Pacific climate processes (Zdanowicz et al. 2014, Osterberg et al. 2017, Winski et al. 2018), if Holocene (or greater) length records can be recovered.

The general timing of deglaciation in Alaska (Brooks Range, Central Alaska Range, and southern Alaska) was determined based on terrestrial cosmogonic radionuclides, lichenometry, and radiocarbon dating to between 10 and 20 ka BP (Dortch 2007). Following the Last Glacial Maximum (LGM), glaciers in the Brooks Range retreated up valley to, or even within, their modern limits by ca. 15 ka (Pendleton et al. 2015). Given the small extent of the Brooks Range glaciers prior to the Holocene thermal maximum, during which some glaciers in southern Alaska disappeared entirely (Barclay et al. 2009), it is possible that the Brooks Range glaciers may have disappeared as well. In the Central Alaska Range, reaching much higher altitudes and considering today's glacier extent, this is rather unlikely. Nevertheless, it is unclear where preserved ice from the early Holocene (or older) can be found in basal layers of these glaciers. Most of the ice cores recovered from the Alaska/Yukon region did not reach bedrock and are thus limited in the time covered, reaching back a few centuries only (Fig. 1). The Prospector

https://doi.org/10.5194/tc-2023-54
Preprint. Discussion started: 8 May 2023

Russel Col (PRCol) ice core from Mt. Logan is an exception, having an estimated bottom age of ~20,000 years based on the assumption that the significant depletion in the water stable isotope ratios observed in the very bottom section of the core is a signal of the LGM cold conditions (Fisher et al. 2008). The PRCol chronology is further constrained by a large $\delta^{18}O$ minimum and coeval increases in deuterium excess and Ca^{2+} which are assigned to the 4.2 ka BP event (Walker et al. 2019), and tephra from the large Alaskan eruption of Aniakchak (3.6 ka BP, Walker et al. 2019). The PRCol record serves as a Global auxiliary stratotype for the Middle/Late Holocene subdivision boundary (Walker et al. 2019). However, there are no chronologic tie points in the PRCol record prior to the 4.2 ka BP event (Walker et al. 2019).

New surface-to-bedrock ice cores were recovered from the Begguya plateau (Mt. Hunter; Denali National Park, Alaska, 62.93°N/151.09°W; Fig. 1) in 2013 at 3900 m elevation (Winski et al. 2017). The two surface-to-bedrock cores (DEN-13A, DEN-13B) reached depths of 211.2 and 209.7 meters, respectively. Analysis of the upper 190 meters of DEN-13B (2013 to 810 CE) revealed that snow accumulation at the drilling site has doubled since ~1840 CE, coeval with warming of western tropical Pacific sea surface temperatures (Winski et al. 2017) and intensification of the Aleutian Low system (Osterberg et al. 2014, Osterberg et al. 2017). The same core also shows a sixty-fold increase in water equivalent of total annual melt between 1850 CE and present, which suggests a summer warming rate of 1.92±0.31°C per century during the last 100 years in the altitude range of 3900 m (Winski et al. 2018). The Begguya melt layer record is significantly correlated with surface temperatures in the central tropical Pacific through a Rossby-wave like pattern that enhances temperatures over Alaska (Winski et al. 2018). Taken together, these hydroclimate changes are consistent with linkages between Pacific decadal variability and Arctic hydroclimate changes seen in the observational record (Svendsen et al. 2018), and demonstrate that the North Pacific hydroclimate response since 1850 CE is unprecedented in the past millennium.

The annual layer counting based chronology of the Denali core results in an ice age of 1203 ± 41 years at a depth of 190 m (152.8 m w.e.; Winski et al. 2017). Below that depth, annual layering was less consistent due to the loss of seasonal resolution caused by the glacier flow-induced thinning of layers. However, based on previously reported depth-age scales of ice cores from cold, high-elevation glaciers frozen to bedrock, the bottom 20 meters of ice may contain most of the record in terms of time, covering the Holocene and potentially even reaching into the Last Glacial (Uglietti et al. 2016, Licciulli et al. 2020). The Denali ice core therefore provides the possibility of establishing a new Holocene North Pacific hydroclimate

https://doi.org/10.5194/tc-2023-54
Preprint. Discussion started: 8 May 2023

record reaching beyond the Common Era, if a precise and absolutely-dated chronology can be established in the bottom 20 meters of the core. The water-insoluble organic carbon (WIOC) and dissolved organic carbon (DOC) ^{14}C-dating method has been validated and applied for multiple mid-latitude ice cores (e.g. Jenk et al. 2009, Uglietti et al. 2016, Hou et al. 2018, Fang et al. 2021). The technique makes use of the transport and deposition of carbonaceous aerosols onto the glacier. Before the industrial period, carbonaceous aerosols were mainly emitted from the living biosphere and from biomass burning. Consequently, this carbon reflects the contemporary atmospheric ^{14}C content (Jenk et al. 2006). After deposition, the WIOC and DOC is incorporated into glacier snow, firn, and ice and undergoes radioactive decay with a half-life of 5730 years (Godwin 1962). Here we report results from ^{14}C analysis of the bottom 60 m of the Denali ice core. These absolute dates extend the existing late Holocene Begguya chronology (Winski et al. 2017), providing the first radiometrically dated high latitude Northern Hemisphere ice core chronology. We discuss our results in relation to Holocene ice extent and climate in the North Pacific region.

2 Methods

2.1 Annual layer counting (ALC)

Two surface-to-bedrock ice cores (DEN-13A, DEN-13B) were drilled in 2013 at 3,900 meters elevation (above sea level) from the saddle between the north and middle peaks of Begguya (Mt. Hunter), Alaska (Winski et al. 2017; Osterberg et al. 2017; Winski et al. 2018; Polashenski et al. 2018). The annual layer counting for DEN-13B, conducted by three researchers independently, was previously published (Winski et al. 2017) and is only briefly described here. The timescale from 2013 to 1777 CE was determined by counting annual oscillations in δ^{18}O (summer peak), melt layers (summer peak), magnesium (spring peak), dust (spring peak), liquid conductivity (summer peak), ammonium (summer peak) and methanesulfonic acid (MSA; late summer-fall peak), consistent with previous North Pacific ice cores (Yasunari et al. 2007, Osterberg et al. 2014, Tsushima et al. 2015). Between 1777 to 1500 CE annual layer counting is based on annual oscillations of δ^{18}O, δD, dust concentration and liquid conductivity that were measured at higher resolution than the other analytes, while conductivity and dust concentrations were exclusively used to date the ice core from 1500 back to 810 CE. For this study, the counting based on these two parameters has been extended back to 339 CE (see Results section 3.2 about Annual layer counting). The Denali ice core chronology is validated from 1750–2013 CE by comparing the timing of peaks in sulfate, chloride and conductivity to

https://doi.org/10.5194/tc-2023-54
Preprint. Discussion started: 8 May 2023

the known dates of explosive volcanic eruptions as well as by using ^{137}Cs as a stratigraphic indicator of nuclear weapons testing (Winski et al. 2017).

2.2 Denali ice core ^{14}C analysis

Sixteen samples were selected from the lower portion of the DEN-13B (Table 1). Because WIOC concentrations at this site were assumed to be low, ice samples of at least 1 kg of mass were cut, aiming for extracted yields of carbon allowing dating with a reasonable uncertainty of 10-20% (> 10 µg C, Uglietti et al. 2016). Samples for WIOC ^{14}C-daing were prepared following the protocol described in Uglietti et al. (2016); a summary is provided here. In order to remove potential contamination in the outer layer of the ice core, pre-cut samples from the inner part of the core were rinsed with ultra-pure water. After melting, the contained carbonaceous particles were filtered onto prebaked quartz fibre filters (Pallflex Tissueqtz-2500QAT-UP). Potential particulate carbonates also remaining on the filter were removed by acidifying three times with 0.5 µL of 0.2 M HCl. These initial steps were performed in a class 100 laminar flow box to ensure clean conditions. At the University of Bern (Laboratory for the Analysis of Radiocarbon with AMS - LARA laboratory) the WIOC samples were then combusted in a thermo-optical OC/EC analyzer (Sunset Modeldoc4L, Sunset Laboratory Inc, USA) with a non-dispersive infrared sensor (NDIR) for CO_2 quantification, using the established Swiss 4S protocol for OC/EC separation (Zhang et al. 2012). Being coupled to a 200 kV compact accelerator mass spectrometer (AMS, mini radiocarbon dating system MICADAS), equipped with a gas ion source and a Gas Interface System (GIS, Ruff et al. 2007, Synal et al. 2007, Szidat et al. 2014), the LARA Sunset-GIS-AMS system (Agrios et al. 2015, Agrios et al. 2017) allowed for final, online ^{14}C measurements of the CO_2 produced from the WIOC fraction.

For the deepest sample from ~209 m depth (Denali 235) the available amount of ice was very limited (~200 g). To ensure sufficient mass of carbon for final AMS analysis, the ^{14}C dating was performed on the DOC fraction for which a higher concentration compared to the WIOC fraction is expected (Legrand et al. 2013). By a catalyzed UV-Oxidation in a dedicated system, DOC was converted to CO_2 which was then cryogenically trapped and flame sealed in glass ampules for final AMS analysis (Fang et al. 2019).

All ^{14}C results are expressed as fraction modern ($F^{14}C$), which is the $^{14}C/^{12}C$ ratio of the sample divided by the same ratio of the modern standard referenced to the year 1950 CE (NIST

https://doi.org/10.5194/tc-2023-54
Preprint. Discussion started: 8 May 2023

standard oxalic acid II, SRM 4990C) both being normalized to -25‰ in $\delta^{13}C$ to account for isotopic fractionation. Daily AMS calibration was performed using sets of modern (NIST oxalic acid II, SRM 4990C, $F^{14}C$ = 1.3407 ± 0.0005) and fossil standards (sodium acetate, Sigma-Aldrich, No. 71180, $F^{14}C$ = 0.0018 ± 0.0005). Final values presented in Table 1 are the AMS $F^{14}C$ raw data after corrections accounting for constant contamination and cross contamination in the Sunset-GIS-AMS system (or GIS-AMS system for DOC, respectively) and the overall procedural blank contribution introduced from preparation of ice samples to final AMS analysis. $F^{14}C$ of DOC was corrected for contribution from ^{14}C in-situ production following Fang et al. (2021). The applied small shift in $F^{14}C$ of 0.019±0.010, was derived using an in-situ production rate of 260.9 ^{14}C atoms per gram ice and year as a best estimate defined for the site latitude and elevation (Lal et al. 1987, Lal and Jull 1990, Lal 1992), an average accumulation rate of 1.0 ± 0.5 m w.e. (Winski et al. 2017), and assuming an average incorporation into DOC of 18±7% (Hoffmann, 2016). To obtain final dates, corrected $F^{14}C$ were calibrated using OxCal v4.4.4 (Ramsey 2021) with IntCal20 (the Northern Hemisphere calibration curve; Reimer et al. 2020) and the OxCal in-built sequence model (Bayesian approach-based deposition model; Ramsey 2008, Ramsey 2017). All calibrated ^{14}C ages are presented as the 1σ range in years before present (cal BP, with BP referring to the year 1950 CE).

3 Results

3.1 Englacial stratigraphy

Around the Begguya drill site, no folding was observed in ground penetrating radar (GPR) data and the bedrock geometry appears to be uncomplicated (Campbell et al. 2013). New radar data was collected in 2022. Ice thickness, bed topography, and internal stratigraphy of the core site were mapped using GPR (10 MHz center frequency radar system, Blue Systems Integration). Standard processing techniques were applied to the data: clipping stationary periods, applying horizontal stacking, bandpass filtering, and correction for antenna separation (Lilien et al. 2020). Data were interpolated for standard trace spacing and then migrated using the SeisUnix sumigtk routine. Clear, visible layering is evident in the majority of the ice column; however, interpretation of the stratigraphy at depth is complicated by sidewall reflections produced from the trough beneath the ice core site. There is no conclusive evidence from this data of either stratigraphic continuity or discontinuity in the bottom-most 10 m of ice (Fig. 2). Future

https://doi.org/10.5194/tc-2023-54
Preprint. Discussion started: 8 May 2023

199 measurements using the millimeter-precision capabilities of autonomous phase sensitive radar
200 (Brennan et al. 2014) would be beneficial to resolve englacial stratigraphy close to the bedrock.

201 **3.2 Annual layer counting**

202 Annual layer counting (ALC), previously published in Winski et al. 2017 back to 810 CE, was
203 extended back to 339 CE (the top 197 meters). The uncertainty in the ALC chronology back to
204 810 CE was estimated through statistical comparisons among individual layer positions
205 indicated by three individuals (see Winski et al. 2017 for details). By 1900 CE, uncertainty
206 estimates are ±4 years, increasing to ±10 years at 1500 CE and ±30 years by 810 CE (190.05
207 m). Only one individual (DW) performed ALC below 190 m, prohibiting a similar approach to
208 estimate uncertainties, but we estimate and uncertainty of around ±60 years at 339 CE. These
209 estimates are for ALC only and do not consider additional, constraining information from time
210 horizons. There is no offset between the timescale and inferred volcanic eruptions as indicated
211 by peaks in sulfate, chloride, and conductivity during the 19th and 20th centuries, indicating
212 that an accuracy within ±2 year throughout the last 200 years is likely. The sulfate and chloride
213 peaks in the 18th century used for chronology validation (inferred as Laki, 1784 CE and Pavlof,
214 1763 CE) were offset by one year from the ALC chronology. Additionally, ^{137}Cs concentrations
215 in the Denali core strongly peak in the layer assigned to the year 1963 CE, one year after the
216 most extensive atmospheric testing of nuclear weapons, which matches the ^{137}Cs residence
217 time in the atmosphere.

218 **3.3 Denali ice core ^{14}C data**

219 Air masses leading to precipitation on Begguya (~3900 m asl.) originate predominantly from
220 the Pacific and contain relatively low organic aerosol concentrations (Haque et al. 2016, Choi
221 et al. 2017). The WIOC concentration in the Denali core is thus significantly lower than in ice
222 cores from the Alps. The WIOC concentrations range from 6 to 31 µg C kg^{-1} ice with an average
223 of 13 ± 7 µg C kg^{-1} (Table 1). This is slightly higher than in Greenland snow at Summit (4.6
224 µg C kg^{-1}, Hagler et al. 2007), but only about half of the pre-industrial WIOC concentrations
225 in European Alpine ice cores, with 24 ± 9 µg C kg^{-1} (Legrand et al. 2007) and 32 ± 18 µg C
226 kg^{-1} (Jenk et al. 2009) from Colle Gnifetti, Monte Rosa, Switzerland and 24 ± 7 µg C kg^{-1} from
227 Fiescherhorn glacier (Jenk et al. 2006). In agreement with findings from previous studies
228 (Legrand et al. 2007), the concentration of DOC (80 µg C kg^{-1}), measured in the deepest sample,
229 was significantly higher than the concentration of WIOC.

https://doi.org/10.5194/tc-2023-54
Preprint. Discussion started: 8 May 2023

^{14}C calibration was performed using the OxCal in-built sequence model (Ramsey, 2008, Ramsey 2017; see *Methods*). The assumption that samples are in chronological order allows statistical constraints for the most likely age distribution of the individual samples in the sequence. This assumption of chronological ordering will be discussed below. Samples containing less than 10 µg carbon are generally characterized by a wide age range. This is expected due to the small carbon amount and the resulting larger analytical uncertainty, related to lower analytical AMS precision as well as to a lower, thus unfavorable signal-to-noise ratio (i.e. the ratio between size of sample and procedural blank, respectively). Although we used a considerable amount of ice for each sample (~1 kg), the total carbon amount in 5 samples was significantly below this 10 µg C threshold recommended to obtain a reliable dating with a final dating uncertainty < 20% (Uglietti et al. 2016). These samples will thus not be discussed in the following (but can be found in the supplement material, together with calibration results without sequence constraint).

Calibrated ^{14}C ages range from 0.3 ± 0.3 ka cal BP at 166.2 m (131.4 m w.e.) depth to 8.4 ± 0.6 ka cal BP for the deepest sample (Denali235; 209.1 m or 169.8 m w.e.), the last sample above bedrock (0.6 m), revealing ice of early Holocene origin in the Denali ice core (Table 1 and Figure 3). The absolute ages from radiocarbon dating are in agreement with the independently derived ages from the annual layer counting reported in Winski et al (2017), extended back to 339 CE in this study (see *Annual layer counting*). For the youngest sample, Denali183 from a depth of 166.2 m (131.4 m w.e.), and Denali 214 from 192.6 m (155.0 m w.e.), the 1σ age range is 4-679 a cal BP and 958-1410 a cal BP, respectively; similar to the respective annual layer counting derived ages of 340-380 and 1200-1410 a BP. The 1σ ^{14}C age range for Denali210-211 at 189.5 m (152.3 m w.e.) is 527-930 a cal BP, which is slightly younger than the annual layer counting derived age of 1020-1200 a BP, but still in agreement within the 2σ uncertainty (317-1174 a cal BP).

Samples of indistinguishable ages, with regards to the achieved dating uncertainty (i.e. analytical precision), were observed in the depth interval from 200.3 to 206.2 m (161.9 to 167.2 m w.e.). This interval corresponds to a time period from around 3.2 to 4.3 ka BP. For the respective samples (Denali223, Denali224-225, Denali229-230, Denali231), a low Agreement Index (denoted as *A* in OxCal) resulted for the applied ^{14}C calibration approach. *A* indicates the level of agreement between the probability function derived by the ordinary calibration approach (a priori distribution) and the calibration with additional constraint (a posterior distribution; see OxCal and Ramsey, 2008 and 2017 for more details). Distributions are shown

https://doi.org/10.5194/tc-2023-54
Preprint. Discussion started: 8 May 2023

in Figure 3. A value of 100 indicates no alteration in the distribution (100% or unity) while a value lower than 60 indicates a warning to check for the validity of the underlying assumption, i.e. (i) a non-sequential layering of samples, or (ii) the presence of analytical outliers. It is apparent from Figure 3, that the two samples with lowest *A* (<10), Denali 223 and 231, are also characterized by an exceptionally large uncertainty. For the batch of samples with AMS Lab ID BE-10013.1.1 to BE-10022.1.1 (Table 1; see also Supplement Figure S1 and Table S1), the contribution to the final overall uncertainty from AMS analysis only was around twice as much than what typically can be achieved for samples of that carbon size. For that measurement day, we also observed above average uncertainties for the measured sets of AMS calibration standards, with a slight elevation in the fossil standard value (+0.02 in $F^{14}C$; see *Method*). This is indication for non-ideal AMS conditions due to sub-optimal instrument tuning on the one hand, and an elevated, potentially non-stable background that day on the other hand. Thus, neither ^{14}C ages nor the englacial stratigraphy give sufficient evidence to conclude a non-sequential ordering of samples (i.e. an age reversal in the Denali ice core). Additionally, there is evidence from other studies from the region suggesting hydrological changes between around 4 to 2 ka BP (e.g. increased lake levels and precipitation, see *Discussion*), which coincides with the time period in question here. Because increased accumulation rates would lead to a reduced increase in age per unit depth, an unambiguous resolving of the sequence then depends on the achievable analytical uncertainty. Having pushed the limit of the analytical method with the small amounts of carbon available for ^{14}C analysis and considering all the above, we thus exclude assumption (i) and are confident that the applied ^{14}C sequence calibration approach does provide us the most accurate dates.

4 Discussion

4.1 Denali ice core chronology

Modeling the age scale in high-elevation mountain ice cores can be attempted either by applying rather simple glaciological one-dimensional (1D) flow models (e.g. Nye 1963, Dansgaard and Johnsen 1969, Bolzan 1985) or by much more complex 3D models based on a suit of observational data from glaciological survey (e.g. Campbell et al. 2013, Licciulli et al. 2020). Independent of model complexity, age scale modeling, particularly of mountain glaciers, is strongly challenged to provide accurate or even conclusive ages along the profile at a specific point on the glacier (e.g. the ice core drill site; Campbell et al. 2013, Licciulli et al. 2020). This is especially the case close to bedrock, where ice flow can become highly complex, and because

https://doi.org/10.5194/tc-2023-54
Preprint. Discussion started: 8 May 2023

295 past annual net accumulation rates with potential variations over time are unknown. Layers of
296 known age along a glacier depth profile, e.g. from ice core dating, can provide crucial model
297 constraints, allowing free model parameters to be tuned for a best fit between observations and
298 model output. For a defined point, moving along a single axis (bed to surface), 1D models
299 benefit from their simplicity to do so (less parameters). 1D models have been applied for
300 decades to obtain continuous age-depth relationships at sites on polar ice sheets (e.g. Dansgaard
301 and Johnsen 1969), thereby also accounting for past changes in accumulation rates by inverse
302 modelling approaches (e.g. Buiron et al. 2011, Buchardt and Dahl-Jensen 2008). However,
303 applications to sites from high-mountain glaciers are more recent (e.g. Jenk et al. 2009, Uglietti
304 et al. 2016).

305 In the case of the Denali ice core, accurate dating by annual layer counting supported
306 with independent time horizons for the upper two thirds of the core and absolute dated horizons
307 for the deep section of the core (^{14}C dates) are available. Winski et al. 2017 developed a well-
308 defined age scale for the upper part of the core based on annual layer counting supported by
309 distinct time horizons. Since depth-age relationships are less challenging to model in the upper
310 90% of the ice core, because of relatively moderate layer thinning and little if any influence
311 from bedrock, Winski et al. (2017) used a combination of 1D modeling and a 3D glacier flow
312 model developed for this site (Campbell et al. 2013) to determine a significant increase in
313 accumulation rates since around 1850 CE. Therefore, significant changes in net accumulation
314 rates at the Denali ice core drill site should be expected to a have also occurred in the more
315 distant past.

316 Due to its simplicity, we used the 1D two-parameter model (2p-model; Bolzan 1985) to
317 provide a first, best estimate for a continuous age-depth relationship from surface to bedrock,
318 building on the available data points presented. The 2p-model is based on a simple analytical
319 expression for the decrease of the annual layer thickness with depth and has two degrees of
320 freedom, the mean annual net accumulation rate b and the thinning parameter p, characterizing
321 the strain rate function; both assumed to be constant over time. Knowing the glacier thickness
322 of 209.7 m from the ice core length (supported by ground penetrating radar data; 170.4 m w.e.)
323 and with all depths converted from meter to meter water equivalent based on the ice core
324 density profile, allowed finding best solutions for b and p by fitting the model (least squares
325 approach, as described in Fahnestock et al. 2001) through the time horizons in the Denali ice
326 core (Volcanos, ^{137}Cs, ^{14}C). The derived value for p was 0.79 ± 0.01. The resulting value of b
327 of 1.5 ± 0.1 m w.e. yr^{-1}, representing the mean annual net accumulation rate for the entire period

https://doi.org/10.5194/tc-2023-54
Preprint. Discussion started: 8 May 2023

328 covered by the ice core, is similar to the recently observed 21st century values. It is however
329 significantly higher than the average value of around 0.5 m w.e. yr^{-1} previously determined for
330 the last 810 years (ranging from around 0.3 to 1.5 m w.e. yr^{-1}; Winski et al. 2017). This is no
331 surprise, considering the likelihood that similar variations may also have occurred further back
332 in time. As a consequence of being constrained by the age of dated layers, the model results
333 are in agreement with the observational data for the total time period covered within the ice
334 column. However, at various depths along the depth profile, a significant offset between model
335 output and data can be observed (Fig. 4a). Again, this is not unexpected, considering the fact
336 that the accumulation rate was kept constant in the model, while significant changes over time
337 are known to have occurred (Winski et al. 2017). In Figure 3a, the effect on model results for
338 variations of *b* is illustrated (runs with b equal to 0.5, 1.5 and 2 m w.e. yr^{-1}, respectively, with
339 *p* as determined before).

340 To achieve our final goal, obtaining a continuous age-depth relationship based on the
341 absolute dating presented, we next applied a simple inverse modeling approach. We tightly fit
342 the model to the experimental data, by numerically solving for the exact value of *b* for each
343 depth with a determined age (*p* and *H* as before). To reduce and account for potential noise in
344 the data, an uncertainty weighted three point running mean to obtain the non-steady state values
345 for *b* was calculated (starting from top, then reversed from bottom, thereby propagating the
346 values for continuity). These values, interpolated for depths between the dated layers, were
347 finally used for model input, yielding a continuous age-depth relationship (Figure 4b and 4c).
348 All uncertainties have been fully propagated throughout calculations (from analysis to
349 modeling). We derive annual net accumulation rates of 0.5±0.1 m w.e. yr^{-1} at around 1000 CE,
350 eventually increasing to a 20th century average value of 1.1±0.2 m w.e. yr^{-1} (Fig. S2). This is
351 in good agreement with what has been determined previously by Winski et al. 2017 for the
352 corresponding periods, based on results from different models investigated (for the 3D model
353 considered best: 0.25 m w.e. yr^{-1} around 1000 CE, with models ranging from 0.05-0.7 m w.e.
354 yr^{-1}, and 1.1±0.3 m w.e. yr^{-1} for the 20th century average, respectively). During the Holocene
355 Climate Optimum (around 8 to 5 ka BP, Kaufman et al. 2016) we obtain net accumulation rates
356 of 1.2±0.3 m w.e. yr^{-1}, similar to the average rate observed since 1950 CE, followed by higher
357 rates of 1.7±0.4 m w.e. yr^{-1} from around 4.3 to 3.2 ka BP. Then, the rates decrease over the
358 next 500 to 1000 years to around 0.4±0.2 m w.e. yr^{-1}. See Section 4.3 for further discussion.
359 Our derived age-depth scale results in ages of 9-14 ka BP at 0.5 m above bedrock, strongly

https://doi.org/10.5194/tc-2023-54
Preprint. Discussion started: 8 May 2023

suggesting the presence of, at least, early Holocene ice to be present at the Denali ice core drill site.

4.2 Ice core chronologies in Eastern Beringia

So far, existing ice cores from Eastern Beringia (Table 2) were dated with ages covering less than the last millennium except for the Denali core discussed in this study and the 188 m long PRCol core (Fig. 1) drilled to bedrock on the summit plateau of Mt. Logan in 2001 and 2002. The older part of the PRCol core was dated based on a signal interpreted as the Younger Dryas to Holocene transition (sudden reduction in electrical conductivity coinciding with a drop in $\delta^{18}O$ and an increase in various chemical species) and a bottom age estimate from an ice flow model of about 20 ka (Fisher et al. 2008). The 152 m ice core drilled in 2008 on the McCall Glacier was dated by using a combination of annual layer counting and specific horizons. The upper 37 m of ice date back to 65 years and the full 152 m core was estimated to cover more than 200 years but no actual dating of the lower section was performed (Klein et al. 2016). The Aurora Peak site is located southeast of Mt. Hayes and the ice core was also drilled in 2008. The total ice thickness at the drilling site is 252±10 m, but this core (180.17 m) did not reach bedrock. By annual layer counting, the estimated bottom age of the Aurora Peak core is about 274 years (Tsushima et al. 2015). Two cores were collected at Eclipse Icefield in 2002. The chronology of these cores is based on multi-parameter annual layer counting of seasonal oscillations in the stable isotope ($\delta^{18}O$) and major ion records (Na^+) supported by identification of volcanic horizons. The longest core 2, 345 m) covers the period 1000 CE to 2002 CE (Yalcin et al. 2007), but did not reach bedrock. In 2004, a 212 m ice core was drilled from Mt. Wrangell. The ice depth in the summit caldera is probably over 900 m, but the definite bottom has not yet been detected (Benson et al. 2007). For this core, no time scale is reported except for a short 12 year record of dust and δD (Yasunari et al. 2007). The record from Mt. Waddington only covers a period of 1973-2010 CE (Neff et al. 2012). The total length of the Mt. Waddington core is 141 m, but the total ice thickness at the drilling site is about 250 m. The ice core from Bona–Churchill reached bedrock at a depth of 460 m, but the age-depth scale has only been established for the last ~800 years (depth of 399 m); the deepest ice is estimated to exceed 1500 years in age (Porter et al. 2019).

Because none of the cores from the Eastern Beringia region was either drilled to bedrock or the ice close to the bed dated by an absolute dating method, no concluding evidence about the age of the oldest glacier ice preserved in this region existed so far. In this study, we achieved

https://doi.org/10.5194/tc-2023-54
Preprint. Discussion started: 8 May 2023

a first, complete and absolute (radiometric) dating by a first application of ^{14}C analysis on a high-latitude Northern Hemisphere ice core from Begguya, which reached down to bedrock. Our results, with calibrated ^{14}C ages of 7.7 to 9.0 ka BP close to the bottom (0.61 m above bedrock) and model based indication for potentially even older ice further below (>12 ka BP), clearly indicate that glaciers in this region can be of early Holocene or even Pleistocene origin. This also confirms that at least some glacier ice in the Central Alaskan Range, at altitudes as low as 3,900 m a.s.l., survived during the Holocene thermal maximum.

4.3 Possible implications for Holocene hydroclimate in Eastern Beringia

The mid-Holocene hydroclimate in the North Pacific has been investigated by various studies previously carried out in the region (Table 3, Fig. 5). For example, the onset of the regional Neoglaciation was estimated to last from around 3.5 to 2.5 ka BP in the Yukon Territory based on past tree line variations (Denton and Karlén 1977, Anderson et al. 2005a) and inferred from lacustrine records of lake level and carbonate oxygen isotopes (Denton and Karlén 1977, Anderson et al. 2005a). Past tree lines also provided evidence for significant glacier extension in the St. Elias Mountains over the period 3.6-3.0 ka BP (Denton and Karlén 1977). While a mid-Holocene temperature decrease may have played a role, Denton and Karlen (1977) hypothesized that an increase in regional precipitation contributed to the regional Neoglaciation. Based on pollen reconstructions, Heusser et al. (1985) inferred a doubling of Southern Alaskan mean annual precipitation from around 3.9 to 3.5 ka BP (Fig. 3). Clegg and Hu (2010) found that effective moisture, particularly during winters, increased markedly between 4.0 and 2.5 ka BP. Hansen and Engstrom (1996) suggest cooler and wetter conditions in Glacier Bay at around 3.4 ka BP. At Jellybean Lake and Marcella Lake, lake levels were high between 2.0-4.0 ka BP (Anderson et al. 2005a, 2005b) which was assigned to changes in the strength and positions of the Aleutian Low (Anderson et al. 2005b), consistent with the more recent interpretation of hydroclimate changes from the Denali ice core (Winski et al. 2017; Osterberg et al. 2017).

The Denali ice core may provide corroborating evidence for a mid-Holocene shift in hydroclimate (Table 3, Fig. 5). As presented before, samples of indistinguishable ages, at least for the achieved analytical precision, were observed in the depth interval from 200.3 to 206.2 m (161.9-167.2 m w.e.) corresponding to the modeled time period from 4.3±0.5 to 3.2±0.5 ka BP (see Sections *Denali ice core ^{14}C data* and *Denali ice core chronology*). While our model results based on ^{14}C ages are consistent with existing interpretations of mid-Holocene changes in regional precipitation, applying other independent dating methods using the remaining

https://doi.org/10.5194/tc-2023-54
Preprint. Discussion started: 8 May 2023

parallel ice sections from this depth interval (e.g. from DEN-13B) could be used, and additional geophysical and modeling approaches are needed to rigorously test this hypothesis.

5 Conclusion

Although ^{14}C analysis of ice-incorporated carbonaceous aerosols has allowed radiocarbon dating of various high-elevation ice cores from low- and mid-latitudes, this technique has not been applied before in high latitude ice cores because of the generally lower carbon content. The ^{14}C results from the Denali ice core are the first from a high latitude ice core. These were achieved by a slight adaptation of the WIOC ^{14}C-dating method, allowing for larger ice samples of up to around 1 kg of ice and the use of a new technique for ^{14}C dating of the DOC fraction (around three times higher in concentration compared to WIOC fraction). Combining dating by annual layer counting to a depth of 197.2 m (159.2 m w.e.; ~1674 years BP or 339 CE, respectively), volcanic tie-points from sulfate, chloride, conductivity, and the new ^{14}C dated horizons, a complete continuous chronology over the entire core was established using a simple inverse ice flow modeling approach. For the overlapping sections, ages based on annual layer counting are confirmed by the agreement with the absolute, radiometric ^{14}C dates.

^{14}C dating of a sample from just 0.61 m above bedrock at around 209 m depth, yielded the first absolute date for near-bedrock ice in the region. Dated to be 7.7 to 9.0 thousand years old, our result clearly indicates this very bottom ice to be of early Holocene age. The additional model results indicate a high likelihood of even older ice below (>12 ka). The old ice at the bottom of the Denali core confirms that at least some glacier ice in the central Alaskan Range survived the Holocene thermal maximum. Future, independent dating methods would be beneficial to further constrain and improve the time scale presented here. Our results show the applicability and great potential of ^{14}C dating on low carbon content samples from North Pacific/Arctic ice cores. While they indicate the Denali ice core to currently be one of the few existing archives in the North Pacific region providing an opportunity to reconstruct Holocene hydroclimate variability, we do expect that similar or even longer paleo ice core records can be recovered from North Pacific glaciers if bedrock can be reached.

Data availability. All ^{14}C data are available in the supplementary material.

Supplementary material. Additional Figures and Tables for this article can be found in the Supplementary.

https://doi.org/10.5194/tc-2023-54
Preprint. Discussion started: 8 May 2023

Author contributions. LF, TMJ and MS performed ^{14}C analysis, evaluation, and the continuous age-depth scale modeling, DW, KK, EO, SC, HLB and CW drilled the core and/or conducted the chemical and physical properties analysis. HLB, DW, and EO identified the annual layers. EE provided the radar image. LF, TMJ, KK and MS wrote the manuscript while all authors contributed to the discussion of the results.

Competing interests. There is no conflict of interest.

Special issue statement. This article is part of the special issue "Ice core science at the three poles (CP/TC inter-journal SI)".

Acknowledgements. Thanks to the Laboratory for the Analysis of Radiocarbon with AMS (LARA) at the University of Bern, especially to Martin Rauber for his help with operating the Sunset-MICADAS system. We thank Denali National Park, Polar Field Services and Talkeetna Air Taxi for providing air support and field assistance, Mike Waszkiewicz for ice core drilling, Brad Markle, Dave Silverstone, Tim Godaire and Elizabeth Burakowski for field assistance, and to more than 25 students for their support in the field and the lab. The work in this manuscript was funded by the U.S. National Science Foundation (AGS-1806422 and AGS-AGS-2002483). FL was supported by State Key Laboratory of Cryospheric Science, Northwest Institute of Eco-Environment and Resources, Chinese Academy Sciences (Grant Number: SKLCS-OP-2021-02).

https://doi.org/10.5194/tc-2023-54
Preprint. Discussion started: 8 May 2023

References

Agrios, K., G. Salazar and S. Szidat, A Continuous-Flow Gas Interface of a Thermal/Optical Analyzer With 14 C AMS for Source Apportionment of Atmospheric Aerosols, Radiocarbon, 2017, 59(3), 921-932.

Agrios, K., G. Salazar, Y.-L. Zhang, C. Uglietti, M. Battaglia, M. Luginbühl, V. G. Ciobanu, M. Vonwiller and S. Szidat, Online coupling of pure O2 thermo-optical methods–14C AMS for source apportionment of carbonaceous aerosols, Nuclear Instruments and Methods in Physics Research Section B: Beam Interactions with Materials and Atoms, 2015, 361, 288-293.

Anderson, L., M. B. Abbott, B. P. Finney and M. E. Edwards, Palaeohydrology of the Southwest Yukon Territory, Canada, based on multiproxy analyses of lake sediment cores from a depth transect, The Holocene, 2005a, 15(8), 1172-1183.

Anderson, L., M. B. Abbott, B. P. Finney and S. J. Burns, Regional atmospheric circulation change in the North Pacific during the Holocene inferred from lacustrine carbonate oxygen isotopes, Yukon Territory, Canada, Quaternary Research, 2005b, 64(1), 21-35.

Barclay, D. J., G. C. Wiles and P. E. Calkin, Holocene glacier fluctuations in Alaska, Quaternary Science Reviews, 2009, 28(21-22), 2034-2048.

Bengtsson, L. S., V. A.; Johannessen, O. M., The Early Twentieth-Century Warming in the Arctic-A Possible Mechanism, Journal of Climate, 2004, 17(20), 4045-4057. DOI: 10.1175/1520-0442(2004)017<4045:tetwit>2.0.co;2.

Benson, C., R. Motyka, S. McNUTT, M. Luethi and M. Truffer, Glacier–volcano interactions in the North Crater of Mt Wrangell, Alaska, Annals of Glaciology, 2007, 45, 48-57.

Blackport, R., J. A. Screen, K. van der Wiel and R. Bintanja, Minimal influence of reduced Arctic sea ice on coincident cold winters in mid-latitudes, Nature Climate Change, 2019, 9(9), 697-704.

Bolzan, J. F., Ice flow at the Dome C ice divide based on a deep temperature profile, Journal of Geophysical Research: Atmospheres, 1985, 90(D5), 8111-8124.

Brennan, P. V., L. B. Lok, K. Nicholls and H. Corr, Phase-sensitive FMCW radar system for high-precision Antarctic ice shelf profile monitoring, IET Radar, Sonar Navigation, 2014, 8(7), 776-786.

Buchardt, S. L. and D. Dahl-Jensen, At what depth is the Eemian layer expected to be found at NEEM?, Annals of glaciology, 2008, 48, 100-102.

Buiron, D., J. Chappellaz, B. Stenni, M. Frezzotti, M. Baumgartner, E. Capron, A. Landais, B. Lemieux-Dudon, V. Masson-Delmotte and M. Montagnat, TALDICE-1 age scale of the Talos Dome deep ice core, East Antarctica, Climate of the Past, 2011, 7(1), 1-16.

Campbell, S., S. Roy, K. Kreutz, S. A. Arcone, E. C. Osterberg and P. Koons, Strain-rate estimates for crevasse formation at an alpine ice divide: Mount Hunter, Alaska, Annals of glaciology, 2013, 54(63), 200-208.

https://doi.org/10.5194/tc-2023-54
Preprint. Discussion started: 8 May 2023

Choi, Y., T. S. Rhee, J. L. Collett Jr, T. Park, S.-M. Park, B.-K. Seo, G. Park, K. Park and T. Lee, Aerosol concentrations and composition in the North Pacific marine boundary layer, Atmospheric Environment, 2017, 171, 165-172.

Clegg, B. F. and F. S. Hu, An oxygen-isotope record of Holocene climate change in the south-central Brooks Range, Alaska, Quaternary Science Reviews, 2010, 29(7-8), 928-939.

Cohen, J., K. Pfeiffer and J. A. Francis, Warm Arctic episodes linked with increased frequency of extreme winter weather in the United States, Nature communications, 2018, 9(1), 869.

Cohen, J., J. A. Screen, J. C. Furtado, M. Barlow, D. Whittleston, D. Coumou, J. Francis, K. Dethloff, D. Entekhabi and J. Overland, Recent Arctic amplification and extreme mid-latitude weather, Nature geoscience, 2014, 7(9), 627-637.

Cohen, J., X. Zhang, J. Francis, T. Jung, R. Kwok, J. Overland, T. Ballinger, U. Bhatt, H. Chen and D. Coumou, Divergent consensuses on Arctic amplification influence on midlatitude severe winter weather, Nature Climate Change, 2019, 1-10.

Dansgaard, W. and S. Johnsen, A flow model and a time scale for the ice core from Camp Century, Greenland, Journal of Glaciology, 1969, 8(53), 215-223.

Denton, G. H. and W. Karlén, Holocene glacial and tree-line variations in the White River Valley and Skolai Pass, Alaska and Yukon Territory, Quaternary Research, 1977, 7(1), 63-111.

Dortch, J. M., Defining the Timing of Glaciation in the Central Alaska Range, Doctoral dissertation, University of Cincinnati, 2007.

Fahnestock, M., W. Abdalati, S. Luo and S. Gogineni, Internal layer tracing and age-depth-accumulation relationships for the northern Greenland ice sheet, Journal of Geophysical Research: Atmospheres, 2001, 106(D24), 33789-33797.

Fang, L., J. Schindler, T. Jenk, C. Uglietti, S. Szidat and M. Schwikowski, Extraction of Dissolved Organic Carbon from Glacier Ice for Radiocarbon Analysis, Radiocarbon, 2019, 61(3), 681-694.

Fang, L., T. M. Jenk, T. Singer, S. Hou and M. Schwikowski, Radiocarbon dating of alpine ice cores with the dissolved organic carbon (DOC) fraction, The Cryosphere, 2021, 15(3), 1537-1550.

Fisher, D., E. Osterberg, A. Dyke, D. Dahl-Jensen, M. Demuth, C. Zdanowicz, J. Bourgeois, R. M. Koerner, P. Mayewski and C. Wake, The Mt Logan Holocene—late Wisconsinan isotope record: tropical Pacific—Yukon connections, The Holocene, 2008, 18(5), 667-677.

Francis, J. A., S. J. Vavrus and J. Cohen, Amplified Arctic warming and mid-latitude weather: new perspectives on emerging connections, Wiley Interdisciplinary Reviews: Climate Change, 2017, 8(5), e474.

Godwin, H., Half-life of radiocarbon, Nature, 1962, 195(4845), 984.

Hagler, G. S., M. H. Bergin, E. A. Smith, J. E. Dibb, C. Anderson and E. J. Steig, Particulate and water-soluble carbon measured in recent snow at Summit, Greenland, Geophysical Research Letters, 2007, 34(16).

https://doi.org/10.5194/tc-2023-54
Preprint. Discussion started: 8 May 2023

549 Hansen, B. C. and D. R. Engstrom, Vegetation history of Pleasant Island, southeastern Alaska,
550 since 13,000 yr BP, Quaternary Research, 1996, 46(2), 161-175.

551 Haque, M. M., K. Kawamura and Y. Kim, Seasonal variations of biogenic secondary organic
552 aerosol tracers in ambient aerosols from Alaska, Atmospheric Environment, 2016, 130, 95-104.

553 Hayward, C., High spatial resolution electron probe microanalysis of tephras and melt
554 inclusions without beam-induced chemical modification. The Holocene, 2012, 22(1), 119–125.
555 https://doi.org/10.1177/0959683611409777

556 Heusser, C. J., L. Heusser and D. Peteet, Late-Quaternary climatic change on the American
557 North Pacific coast, Nature, 1985, 315(6019), 485-487.

558 Hou, S., T. M. Jenk, W. Zhang, C. Wang, S. Wu, Y. Wang, H. Pang and M. Schwikowski, Age
559 ranges of the Tibetan ice cores with emphasis on the Chongce ice cores, western Kunlun
560 Mountains, The Cryosphere, 2018, 12(7), 2341-2348.

561 Iverson, N. A., D. Kalteyer, N. W. Dunbar, A. Kurbatov and M. Yates, Advancements and best
562 practices for analysis and correlation of tephra and cryptotephra in ice, Quaternary
563 Geochronology, 2017, 40, 45-55.

564 Jenk, T. M., S. Szidat, M. Schwikowski, H. W. Gaggeler, S. Brutsch, L. Wacker, H. A. Synal
565 and M. Saurer, Radiocarbon analysis in an Alpine ice core: record of anthropogenic and
566 biogenic contributions to carbonaceous aerosols in the past (1650-1940), Atmospheric
567 Chemistry and Physics, 2006, 6, 5381-5390.

568 Jenk, T. M., S. Szidat, D. Bolius, M. Sigl, H. W. Gaeggeler, L. Wacker, M. Ruff, C. Barbante,
569 C. F. Boutron and M. Schwikowski, A novel radiocarbon dating technique applied to an ice
570 core from the Alps indicating late Pleistocene ages, Journal of Geophysical Research:
571 Atmospheres, 2009, 114(D14).

572 Kaufman, D. S., Y. L. Axford, A. C. Henderson, N. P. McKay, W. W. Oswald, C. Saenger, R.
573 S. Anderson, H. L. Bailey, B. Clegg and K. Gajewski, Holocene climate changes in eastern
574 Beringia (NW North America)–A systematic review of multi-proxy evidence, Quaternary
575 Science Reviews, 2016, 147, 312-339.

576 Klein, E., M. Nolan, J. McConnell, M. Sigl, J. Cherry, J. Young and J. Welker, McCall Glacier
577 record of Arctic climate change: Interpreting a northern Alaska ice core with regional water
578 isotopes, Quaternary Science Reviews, 2016, 131, 274-284.

579 Lal, D., Cosmogenic in situ radiocarbon on the earth. Radiocarbon After Four Decades,
580 Springer**,** 1992,146-161.

581 Lal, D., K. Nishiizumi and J. Arnold, In situ cosmogenic ^{3}H, ^{14}C, and ^{10}Be for determining the
582 net accumulation and ablation rates of ice sheets, Journal of Geophysical Research: Solid Earth,
583 1987, 92(B6), 4947-4952.

584 Lal, D. and A. Jull, On determining ice accumulation rates in the past 40,000 years using in
585 situ cosmogenic ^{14}C, Geophysical Research Letters, 1990, 17(9), 1303-1306.

586 Legrand, M., S. Preunkert, M. Schock, M. Cerqueira, A. Kasper-Giebl, J. Afonso, C. Pio, A.
587 Gelencsér and I. Dombrowski-Etchevers, Major 20th century changes of carbonaceous aerosol
588 components (EC, WinOC, DOC, HULIS, carboxylic acids, and cellulose) derived from Alpine
589 ice cores, Journal of Geophysical Research, 2007, 112(D23). DOI: 10.1029/2006jd008080.

https://doi.org/10.5194/tc-2023-54
Preprint. Discussion started: 8 May 2023

590 Legrand, M., S. Preunkert, B. May, J. Guilhermet, H. Hoffman and D. Wagenbach, Major 20th
591 century changes of the content and chemical speciation of organic carbon archived in Alpine
592 ice cores: Implications for the long-term change of organic aerosol over Europe, Journal of
593 Geophysical Research: Atmospheres, 2013, 118(9), 3879-3890.

594 Licciulli, C., P. Bohleber, J. Lier, O. Gagliardini, M. Hoelzle and O. Eisen, A full Stokes ice-
595 flow model to assist the interpretation of millennial-scale ice cores at the high-Alpine drilling
596 site Colle Gnifetti, Swiss/Italian Alps, Journal of Glaciology, 2020, 66(255), 35-48.

597 Lilien, D. A., B. H. Hills, J. Driscol, R. Jacobel and K. Christianson, ImpDAR: an open-source
598 impulse radar processor, Annals of Glaciology, 2020, 61(81), 114-123.

599 Neff, P. D., E. J. Steig, D. H. Clark, J. R. McConnell, E. C. Pettit and B. Menounos, Ice-core
600 net snow accumulation and seasonal snow chemistry at a temperate-glacier site: Mount
601 Waddington, southwest British Columbia, Canada, Journal of Glaciology, 2012, 58(212),
602 1165-1175. DOI: 10.3189/2012JoG12J078.

603 Nye, J., On the theory of the advance and retreat of glaciers, Geophysical Journal International,
604 1963, 7(4), 431-456.

605 Osterberg, E. C., P. A. Mayewski, D. A. Fisher, K. J. Kreutz, K. A. Maasch, S. B. Sneed and
606 E. Kelsey, Mount Logan ice core record of tropical and solar influences on Aleutian Low
607 variability: 500–1998 A.D, Journal of Geophysical Research: Atmospheres, 2014, 119(19),
608 2014JD021847. DOI: 10.1002/2014JD021847.

609 Osterberg, E. C., D. A. Winski, K. J. Kreutz, C. P. Wake, D. G. Ferris, S. Campbell, D. Introne,
610 M. Handley and S. Birkel, The 1200 year composite ice core record of Aleutian Low
611 intensification, Geophysical Research Letters, 2017, 44(14), 7447-7454. DOI:
612 10.1002/2017GL073697.

613 Park, H.-S., S.-J. Kim, A. L. Stewart, S.-W. Son and K.-H. Seo, Mid-Holocene Northern
614 Hemisphere warming driven by Arctic amplification, Science Advances, 2019, 5(12),
615 eaax8203.

616 Pendleton, S. L., E. G. Ceperley, J. P. Briner, D. S. Kaufman and S. Zimmerman, Rapid and
617 early deglaciation in the central Brooks Range, Arctic Alaska, Geology, 2015, 43(5), 419-422.

618 Polashenski, D. J., E. C. Osterberg, B. G. Koffman, D. Winski, K. Stamieszkin, K. J. Kreutz,
619 C. P. Wake, D. G. Ferris, D. Introne and S. Campbell, Denali ice core methanesulfonic acid
620 records North Pacific marine primary production, Journal of Geophysical Research:
621 Atmospheres, 2018, 123(9), 4642-4653.

622 Porter, S. E., E. Mosley-Thompson and L. G. Thompson, Ice core $\delta^{18}O$ record linked to
623 Western Arctic sea ice variability, Journal of Geophysical Research: Atmospheres, 2019,
624 124(20), 10784-10801.

625 Ramsey, C. B., Deposition models for chronological records, Quaternary Science Reviews,
626 2008, 27(1-2), 42-60.

627 Ramsey, C. B., Methods for summarizing radiocarbon datasets, Radiocarbon, 2017, 59(6),
628 1809-1833.

629 Ramsey, C. B., OxCal 4.4.4 calibration program. Website: https://c14. arch. ox. ac.
630 uk/oxcal/OxCal. html, 2021.

https://doi.org/10.5194/tc-2023-54
Preprint. Discussion started: 8 May 2023

631 Reimer, P. J., W. E. Austin, E. Bard, A. Bayliss, P. G. Blackwell, C. B. Ramsey, M. Butzin, H.
632 Cheng, R. L. Edwards and M. Friedrich, The IntCal20 Northern Hemisphere radiocarbon age
633 calibration curve (0–55 cal kBP), Radiocarbon, 2020, 62(4), 725-757.

634 Ruff, M., L. Wacker, H. Gäggeler, M. Suter, H.-A. Synal and S. Szidat, A gas ion source for
635 radiocarbon measurements at 200 kV, Radiocarbon, 2007, 49(2), 307-314.

636 Screen, J. A. and J. A. Francis, Contribution of sea-ice loss to Arctic amplification is regulated
637 by Pacific Ocean decadal variability, Nature Climate Change, 2016, 6(9), 856.

638 Screen, J. A., C. Deser, D. M. Smith, X. Zhang, R. Blackport, P. J. Kushner, T. Oudar, K. E.
639 McCusker and L. Sun, Consistency and discrepancy in the atmospheric response to Arctic sea-
640 ice loss across climate models, Nature Geoscience, 2018, 11(3), 155-163.

641 Solomina, O. N., R. S. Bradley, D. A. Hodgson, S. Ivy-Ochs, V. Jomelli, A. N. Mackintosh, A.
642 Nesje, L. A. Owen, H. Wanner and G. C. Wiles, Holocene glacier fluctuations, Quaternary
643 Science Reviews, 2015, 111, 9-34.

644 Svendsen, L., N. Keenlyside, I. Bethke, Y. Gao and N.-E. Omrani, Pacific contribution to the
645 early twentieth-century warming in the Arctic, Nature Climate Change, 2018, 8(9), 793.

646 Synal, H.-A., M. Stocker and M. Suter, MICADAS: a new compact radiocarbon AMS system,
647 Nuclear Instruments and Methods in Physics Research Section B: Beam Interactions with
648 Materials and Atoms, 2007, 259(1), 7-13.

649 Szidat, S., G. A. Salazar, E. Vogel, M. Battaglia, L. Wacker, H.-A. Synal and A. Türler, ^{14}C
650 analysis and sample preparation at the new Bern Laboratory for the Analysis of Radiocarbon
651 with AMS (LARA), Radiocarbon, 2014, 56(2), 561-566.

652 Tokinaga, H., S.-P. Xie and H. Mukougawa, Early 20th-century Arctic warming intensified by
653 Pacific and Atlantic multidecadal variability, Proceedings of the National Academy of Sciences,
654 2017, 114(24), 6227-6232.

655 Tsushima, A., S. Matoba, T. Shiraiwa, S. Okamoto, H. Sasaki, D. J. Solie and K. Yoshikawa,
656 Reconstruction of recent climate change in Alaska from the Aurora Peak ice core, central
657 Alaska, Clim. Past, 2015, 11(2), 217-226. DOI: 10.5194/cp-11-217-2015.

658 Uglietti, C., A. Zapf, T. M. Jenk, M. Sigl, S. Szidat, G. Salazar and M. Schwikowski,
659 Radiocarbon dating of glacier ice: overview, optimisation, validation and potential, The
660 Cryosphere, 2016, 10(6), 3091-3105. DOI: 10.5194/tc-10-3091-2016.

661 Walker, M., M. J. Head, J. Lowe, M. Berkelhammer, S. BjÖrck, H. Cheng, L. C. Cwynar, D.
662 Fisher, V. Gkinis and A. Long, Subdividing the Holocene Series/Epoch: formalization of
663 stages/ages and subseries/subepochs, and designation of GSSPs and auxiliary stratotypes,
664 Journal of Quaternary Science, 2019, 34(3), 173-186.

665 Winski, D., E. Osterberg, D. Ferris, K. Kreutz, C. Wake, S. Campbell, R. Hawley, S. Roy, S.
666 Birkel, D. Introne and M. Handley, Industrial-age doubling of snow accumulation in the Alaska
667 Range linked to tropical ocean warming, Scientific Reports, 2017, 7(1), 17869. DOI:
668 10.1038/s41598-017-18022-5.

669 Winski, D., E. Osterberg, K. Kreutz, C. Wake, D. Ferris, S. Campbell, M. Baum, A. Bailey, S.
670 Birkel and D. Introne, A 400-Year Ice Core Melt Layer Record of Summertime Warming in
671 the Alaska Range, Journal of Geophysical Research: Atmospheres, 2018, 123(7), 3594-3611.

https://doi.org/10.5194/tc-2023-54
Preprint. Discussion started: 8 May 2023

672 Yalcin, K., C. P. Wake, K. J. Kreutz, M. S. Germani and S. I. Whitlow, Ice core paleovolcanic
673 records from the St. Elias Mountains, Yukon, Canada, Journal of Geophysical Research:
674 Atmospheres, 2007, 112(D8).

675 Yasunari, T. J., T. Shiraiwa, S. Kanamori, Y. Fujii, M. Igarashi, K. Yamazaki, C. S. Benson
676 and T. Hondoh, Intra-annual variations in atmospheric dust and tritium in the North Pacific
677 region detected from an ice core from Mount Wrangell, Alaska, Journal of Geophysical
678 Research: Atmospheres, 2007, 112(D10).

679 Zdanowicz, C., D. Fisher, J. Bourgeois, M. Demuth, J. Zheng, P. Mayewski, K. Kreutz, E.
680 Osterberg, K. Yalcin and C. Wake, Ice cores from the St. Elias Mountains, Yukon, Canada:
681 their significance for climate, atmospheric composition and volcanism in the North Pacific
682 region, Arctic, 2014, 35-57.

683 Zhang, Y. L., N. Perron, V. G. Ciobanu, P. Zotter, M. C. Minguillón, L. Wacker, A. S. H.
684 Prévôt, U. Baltensperger and S. Szidat, On the isolation of OC and EC and the optimal strategy
685 of radiocarbon-based source apportionment of carbonaceous aerosols, Atmospheric Chemistry
686 and Physics, 2012, 12, 10841-10856.

687

688

https://doi.org/10.5194/tc-2023-54
Preprint. Discussion started: 8 May 2023

The Cryosphere
Discussions
Open Access
EGU

Table 1 ^{14}C results of the Denali ice core samples (DEN-13B), given as $F^{14}C$, ^{14}C ages, and calibrated ^{14}C ages. For ^{14}C calibration, chronological layering was assumed (sequential deposition, see main text). Samples were dated using the WIOC fraction, except for section 235 in which the DOC fraction was analysed. Numbers of the carbon amount available for ^{14}C AMS analysis as well as the concentration of WIOC (DOC) in the sample are also provided. Additionally shown is the range of the dating based on ALC (range from top to bottom depth of section) and the final age scale (inverse ice flow model).

Sample ID	AMS Lab ID	Depth (m)	Mid Depth (m w.e.)	Carbon amount (µg C)	WIOC (µg kg^{-1})	$F^{14}C$ (1σ)	^{14}C age (a BP, 1σ)	Calibrated ^{14}C age (a cal BP, 1σ range)	Final age scale (a BP)	ALC (a BP)
Denali164	BE-10013.1.1	148.6-149.4	115.90	7.0	6.2	0.910± 0.058	758 ± 513	-*	160-180	150-180
Denali183	BE-10015.1.1	165.7-166.6	131.40	10.8	10.1	0.921± 0.042	661 ± 367	4-679	350-370	340-380
Denali209	BE-10016.1.1	187.8-188.7	151.16	9.2	9.8	0.826± 0.044	1536 ± 428	-*	1010-1060	980-1090
Denali210-211	BE-8997.1.1	188.7-190.3	152.29	10.8	20.0	0.922 ± 0.033	652 ± 288	527-930	1080-1130	1030-1190
Denali214	BE-10017.1.1	192.1-192.9	155.00	13.7	11.8	0.831± 0.036	1487 ± 348	958-1410	1160-1420	1230-1380
Denali215-216	BE-8998.1.1	193.0-194.7	156.17	8.8	12.0	0.925± 0.039	626 ± 339	-*	1200-1560	1290-1500
Denali217	BE-10018.1.1	194.7-195.5	157.33	6.7	6.1	0.731± 0.054	2517 ± 594	-*	1280-1710	1400-1560
Denali219-220	BE-8615.1.1	196.4-197.3	159.31	12.0	16.8	0.841± 0.026	1391 ± 248	1242-1706	1560-1970	>1420
Denali223	BE-10019.1.1	199.8-200.7	161.93	21.4	17.3	0.608± 0.029	3997 ± 383	3079-3469	2180-2890	-
Denali224-225	BE-11923.1.1	200.7-202.3	163.06	33.9	17.5	0.653± 0.010	3423 ± 123	3257-3530	2470-3510	-
Denali228	BE-10020.1.1	203.5-204.2	165.11	8.7	10.0	0.627± 0.043	3750 ± 552	-*	2860-3850	-
Denali229-230	BE-11924.1.1	204.2-205.7	166.09	38.6	20.0	0.691± 0.009	2969 ± 105	3305-3566	3040-4040	-
Denali231	BE-10021.1.1	205.7-206.6	167.18	11.3	11.5	0.523± 0.037	5207 ± 569	3840-4263	3540-4560	-
Denali232-233	BE-11925.1.1	206.6-208.1	168.26	54.8	30.8	0.629± 0.008	3724 ± 102	4067-4407	4520-5430	-
Denali234	BE-10022.1.1	208.1-208.8	169.23	9.8	11.7	0.378± 0.043	7814 ± 918	7264-8406	6270-9650	-
Denali235#	BE-12465.1.1	208.8-209.4	169.83	20.7	80.3$_{DOC}$	(0.437± 0.025) 0.418± 0.027$^{\$}$	6649 ± 447 7007 ± 520	7737-8987$^{\$}$	8920-13140	-

*Following recommendations, samples with a carbon mass of significantly less than 10 µg C were not considered (Uglietti et al. 2016).
#Results from the DOC fraction.
$After correction for in-situ ^{14}C production (Fang et al. 2021; see main text).

https://doi.org/10.5194/tc-2023-54
Preprint. Discussion started: 8 May 2023

700 **Table 2** Overview of existing North Pacific ice cores.

Site	Year of drilling (CE)	Latitude (°N)	Longitude (°W)	Elevation (m asl.)	Depth (m)	Reported time span (a)
McCall Glacier[a]	2008	69.17	143.47	2310	152	>200
Aurora Peak[b]	2008	63.52	146.54	2825	180	~274
Begguya[c]	2013	62.56	151.05	3900	208	>8'000
Mt. Wrangell[d]	2004	62	144	4100	212	~12
Bona-Churchill[e]	2002	61.40	141.42	4420	461	~800
Mt. Logan PRCol[f]	2001-2002	60.59	140.50	5340	188	~20'000
Eclipse Icefield[g]	2002	60.51	139.47	3017	345	~1'000
Mt. Waddington[h]	2010	51.38	125.26	3000	141	~40

701

702 [a]McCall Glacier (Klein et al. 2016), [b]Aurora Peak (Tsushima et al. 2015), [c]Begguya (this study), [d]Mt.
703 Wrangell (Yasunari et al. 2007), [e]Bona-Churchill (Porter et al. 2019), [f]Mt. Logan (Fisher et al. 2008),
704 [g]Eclipse Icefiled (Yalcin et al. 2007),[h]Mt. Waddington (Neff et al. 2012)

705

706 **Table 3** Regional paleoclimate events.

Location	Reference	Paleoclimate events	Time (ka BP)
Begguya	this study	Elevated net accumulation rates	4.3±0.5 to 3.2±0.5
Yukon Territory	Denton and Karlén 1977; Anderson et al. 2005	Neoglaciation	3.5 to 2.5
St. Elias Mountains	Denton and Karlén 1977	Glacier extension	3.6 to 3.0
Southern Alaskan	Heusser et al. 1985	Precipitation increase	3.9 to 3.5
Jellybean Lake	Anderson et al. 2005a	Lake level increase	4.0 to 2.0
Marcella Lake	Anderson et al. 2005b	Lake level increase	4.0 to 2.0
Takahula Lake	Clegg and Hu 2010	Moisture increase	4.0 to 2.5
Alaska	Solomina et al. 2015	Glacier extension	3.5 to 3.0

707

708 .

https://doi.org/10.5194/tc-2023-54
Preprint. Discussion started: 8 May 2023

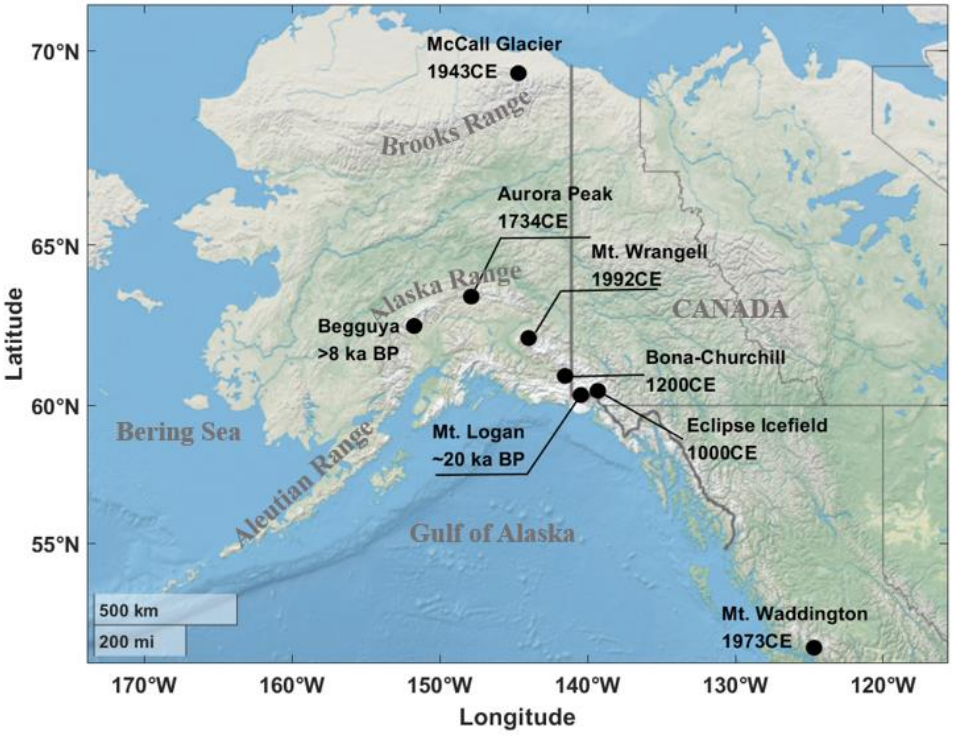

709

710 **Figure 1** Location map of North Pacific ice core sites and the age of the oldest ice dated from
711 each location: Begguya (Mt. Hunter; this study), McCall Glacier (Klein et al. 2016), Aurora
712 Peak (Tsushima et al. 2015), Mt. Wrangell (Yasunari et al. 2007), Bona-Churchill (Porter et al.
713 2019), Mt. Logan (Fisher et al. 2008), Eclipse Icefield (Yalcin et al. 2007), and Mt. Waddington
714 (Neff et al. 2012). The map was produced using MATLAB (R2019b).

715

716

https://doi.org/10.5194/tc-2023-54
Preprint. Discussion started: 8 May 2023

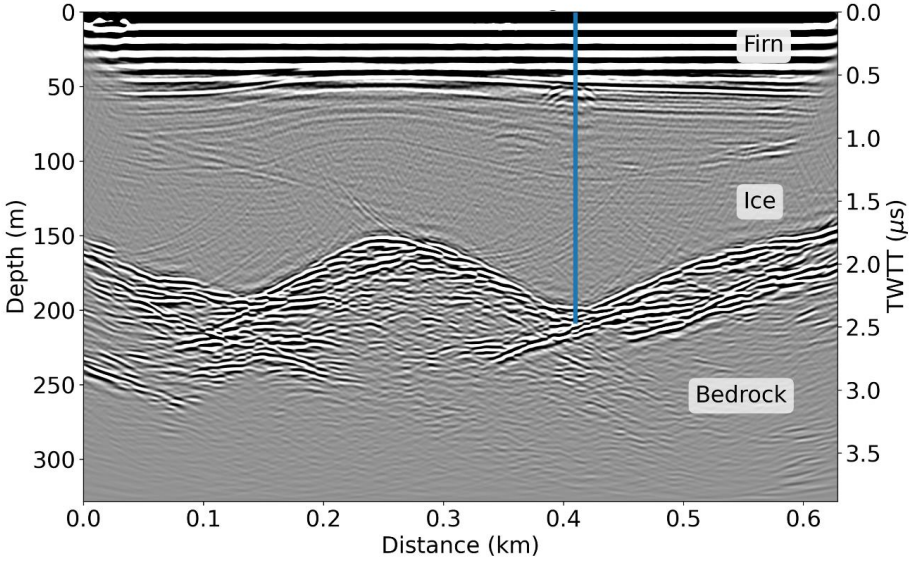

Figure 2 Ground penetrating radar profile collected with 10 MHz BSI radar across the Begguya plateau in 2022. Standard processing techniques were applied to the data using ImpDAR (Lilien et al. 2020). The Two-Way Travel Time (TWTT) is plotted on the y-axis on the right side. The Denali ice core drilling (DEN-13B) is indicated by the vertical blue line.

https://doi.org/10.5194/tc-2023-54
Preprint. Discussion started: 8 May 2023

722

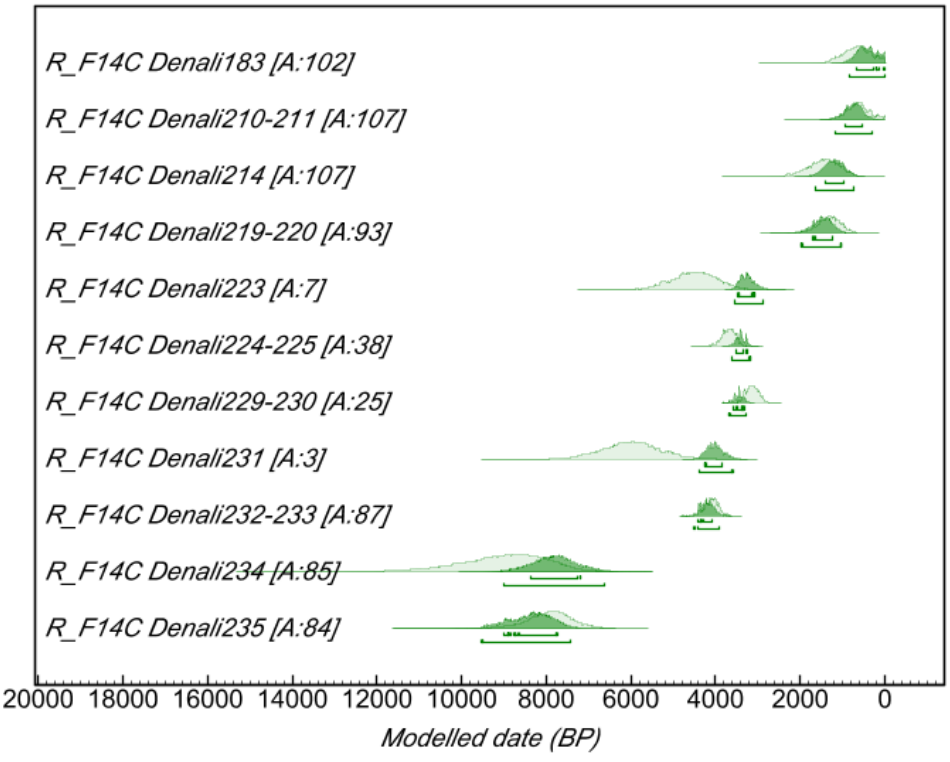

723

724 **Figure 3** Calibrated ^{14}C age probability distributions for samples from the Denali ice core
725 (DEN-13B). as derived in OxCal v4.4.4 using the IntCal 20 radiocarbon calibration curve
726 (Ramsey 2021, Reimer et al. 2020). Light green areas indicate the priori age probabilities, the
727 dark green areas the posterior probabilities when sequential ordering of samples is assumed
728 (see main text). The Agreement Index (*A*) indicates overlap between these two probability
729 functions. *A* value < 60 indicates poor agreement (see main text). The 1σ and 2σ range is
730 indicated by the lines below the probability distribution areas.

731

https://doi.org/10.5194/tc-2023-54
Preprint. Discussion started: 8 May 2023

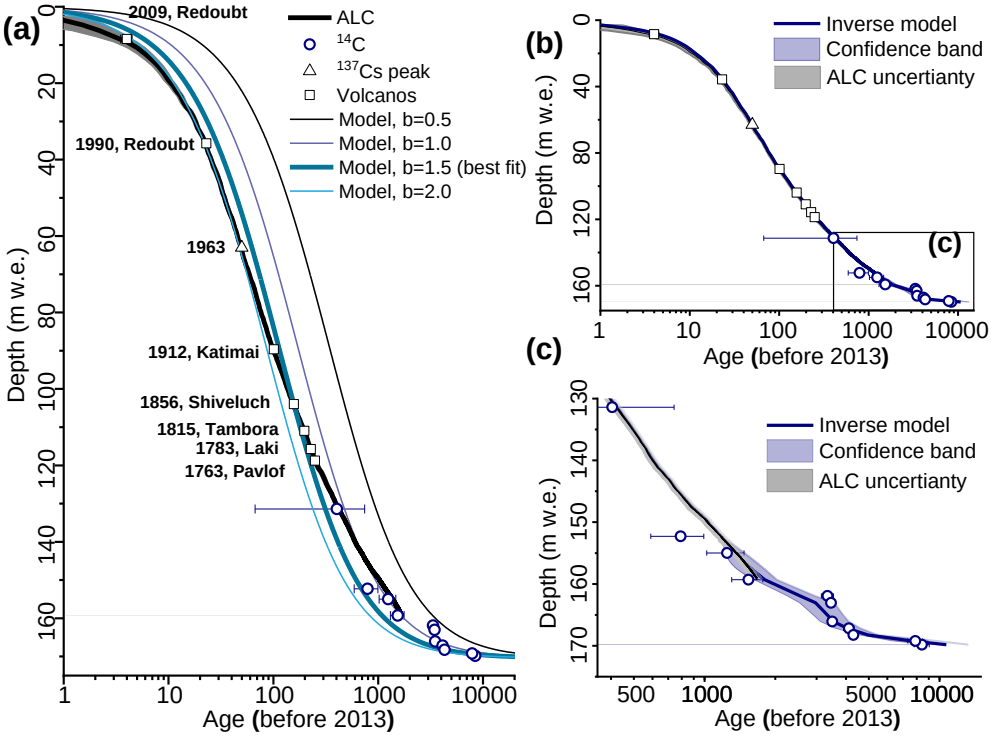

732

733 **Figure 4** Denali ice core (DEN-13B): annual layer counting (ALC), dating horizons (^{14}C,
734 Volcanos, ^{137}Cs peak) and modeled, continuous age-depth relationship (1D ice flow model, see
735 main text). (a) Model output for constant accumulation rates (*b*, in m w.e. yr^{-1}). (b) Modeled
736 age-depth relationship for variable *b* (inverse model). (c) Zoom of the deepest part. All error
737 bars indicate the 1σ uncertainty.

738

739

https://doi.org/10.5194/tc-2023-54
Preprint. Discussion started: 8 May 2023

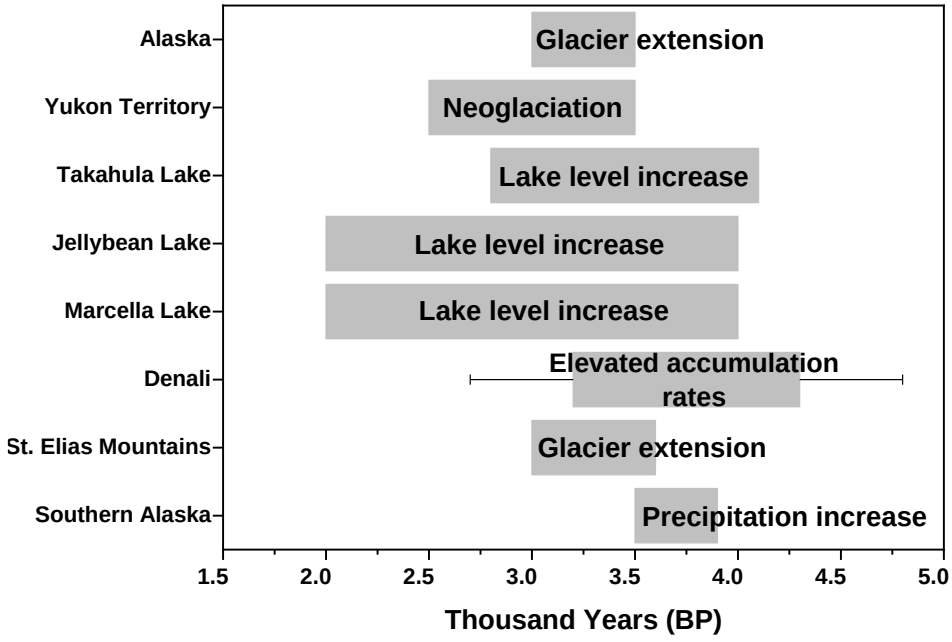

740

741 **Figure 5** Regional paleoclimate changes as reported in previous studies (Anderson et al. 2005a,
742 2005b, Clegg and Hu 2010, Denton and Karlén 1977, Heusser et al. 1985, Solomina et al. 2015)
743 and the period of elevated annual net accumulation rates indicated in the Denali ice core DEN-
744 13B (this study, see main text).

745